UTAS–PHYS–96–44
OUT–4102–64
MZ–TH/96–25
revised November 14, 1996
change to Eq (7)
change to item 1. of conclusions
update to refs. [6,9,10,14]

Association of multiple zeta values with positive knots via Feynman diagrams up to 9 loops*)

D. J. Broadhurst[1)] and **D. Kreimer**[2)]

Department of Physics, University of Tasmania,
GPO Box 252C, Hobart, Tasmania 7001, Australia

Abstract It is found that the number, M_n, of irreducible multiple zeta values (MZVs) of weight n, is generated by $1 - x^2 - x^3 = \prod_n (1 - x^n)^{M_n}$. For $9 \geq n \geq 3$, M_n enumerates positive knots with n crossings. Positive knots to which field theory assigns knot-numbers that are not MZVs first appear at 10 crossings. We identify all the positive knots, up to 15 crossings, that are in correspondence with irreducible MZVs, by virtue of the connection between knots and numbers realized by Feynman diagrams with up to 9 loops.

*) Work supported in part by grant CHRX–CT94–0579, from HUCAM.
1) D.Broadhurst@open.ac.uk; on leave of absence from the Open University, UK.
2) kreimer@dipmza.physik.uni-mainz.de; on leave of absence from Mainz University, FRG.

1. Introduction

The connection of positive knots with transcendental numbers, via the counterterms of quantum field theory, proposed in [1] and developed in [2], and has been vigorously tested against previous [3, 4] and new [5] calculations, entailing knots with up to 11 crossings, related by counterterms with up to 7 loops to numbers that are irreducible multiple zeta values (MZVs) [6, 7]. Cancellations of transcendentals in gauge theories have been illuminated by knot theory [8]. All-order results, from large-N analyses [9] and Dyson-Schwinger methods [10], have further strengthened the connection of knot theory and number theory, via field theory. A striking feature of this connection is that the first irreducible MZV of depth 2 occurs at weight 8 [4, 11], in accord with the appearance of the first positive 3-braid knot at crossing number 8. Likewise the first irreducible MZV of depth 3 occurs at weight 11 [12], matching the appearance of the first positive 4-braid at 11 crossings, obtained from skeining link diagrams that encode momentum flow in 7-loop counterterms [5]. Moreover, the investigations in [9] led to a new discovery at weight 12, where it was found that the reduction of MZVs first entails alternating Euler sums. The elucidation of this phenomenon resulted in an enumeration [13] of irreducible Euler sums and prompted intensive searches for evaluations of sums of arbitrary depth [14]. A review of all these developments is in preparation [15].

This paper pursues the connection to 8 and 9 loops, entailing knots with up to 15 crossings. In Section 2, we enumerate irreducible MZVs by weight. Section 3 reports calculations of Feynman diagrams that yield transcendental knot-numbers entailing MZVs up to weight 15. In Section 4 we enumerate positive knots, up to 15 crossings, and give the braid words and HOMFLY polynomials [16] for all knots associated with irreducible MZVs of weight $n < 17$. Section 5 gives our conclusions.

2. Multiple zeta values

We define k-fold Euler sums [11, 12] as in [13, 14], allowing for alternations of signs in

$$\zeta(s_1, \ldots, s_k; \sigma_1, \ldots, \sigma_k) = \sum_{n_j > n_{j+1} > 0} \prod_{j=1}^{k} \frac{\sigma_j^{n_j}}{n_j^{s_j}}\,, \tag{1}$$

where $\sigma_j = \pm 1$, and the exponents s_j are positive integers, with $\sum_j s_j$ referred to as the weight (or level) and k as the depth. We combine the strings of exponents and signs into a single string, with s_j in the jth position when $\sigma_j = +1$, and $\overline{s}_j$ in the jth position when $\sigma_j = -1$. Referring to non-alternating sums as MZVs [6], we denote the numbers of irreducible Euler sums and MZVs by E_n and M_n, at weight n, and find that

$$1 - x - x^2 = \prod_{n>0} (1 - x^n)^{E_n}\,; \quad 1 - x^2 - x^3 = \prod_{n>0} (1 - x^n)^{M_n}\,, \tag{2}$$

whose solutions, developed in Table 1, are given in closed form by

$$E_n = \frac{1}{n} \sum_{d|n} \mu(n/d) L_d\,; \qquad L_n = L_{n-1} + L_{n-2}\,; \quad L_1 = 1\,; \quad L_2 = 3\,, \tag{3}$$

$$M_n = \frac{1}{n} \sum_{d|n} \mu(n/d) P_d\,; \qquad P_n = P_{n-2} + P_{n-3}\,; \quad P_1 = 0\,; \quad P_2 = 2; \quad P_3 = 3\,, \tag{4}$$

where μ is the Möbius function, L_n is a Lucas number [13] and P_n is a Perrin number [17].

Table 1: The integer sequences (3,4,8) for $n \leq 20$.

n	1	2	3	4	5	6	7	8	9	10	11	12	13	14	15	16	17	18	19	20
E_n	1	1	1	1	2	2	4	5	8	11	18	25	40	58	90	135	210	316	492	750
M_n	0	1	1	0	1	0	1	1	1	1	2	2	3	3	4	5	7	8	11	13
K_n	0	0	1	0	1	1	1	2	2	3	4	5	7	9	12	16	21	28	37	49

In [13], $E_n = \sum_k E_{n,k}$ was apportioned, according to the minimum depth k at which irreducibles of weight n occur. Similarly, we have apportioned $M_n = \sum_k M_{n,k}$. The results are elements of Euler's triangle [13]

$$T(a,b) = \frac{1}{a+b} \sum_{d|a,b} \mu(d)\, P(a/d, b/d)\,, \tag{5}$$

which is a Möbius transform of Pascal's triangle, $P(a,b) = \binom{a+b}{a} = P(b,a)$. We find that

$$E_{n,k} = T(\tfrac{n-k}{2}, k)\,; \quad M_{n,k} = T(\tfrac{n-3k}{2}, k)\,, \tag{6}$$

for $n > 2$ and $n + k$ even. There is a remarkable feature of the result for $M_{n,k}$: it gives the number of irreducible Euler sums of weight n and depth k that occur in the reduction of MZVs, which is *not* the same as the number of irreducible MZVs of this weight and depth. It was shown in [9, 13] that alternating multiple sums occur in the reduction of non-alternating multiple sums. For example, $\zeta(4,4,2,2)$ cannot be reduced to MZVs of lesser depth, but it can [13] be reduced to the alternating Euler sum $\zeta(\overline{9},\overline{3})$. Subsequently we found that an analogous "pushdown" occurs at weight 15, where depth-5 MZVs, such as $\zeta(6,3,2,2,2)$, cannot be reduced to MZVs of lesser depth, yet can be reduced to alternating Euler sums, with $\zeta(9,\overline{3},\overline{3}) - \frac{3}{14}\zeta(7,\overline{5},\overline{3})$ serving as the corresponding depth-3 irreducible. We conjecture that the number, $D_{n,k}$, of MZVs of weight n and depth k that are not reducible to MZVs of lesser depth is generated by

$$1 - \frac{x^3 y}{1-x^2} + \frac{x^{12} y^2 (1-y^2)}{(1-x^4)(1-x^6)} = \prod_{n\geq 3} \prod_{k \geq 1} (1 - x^n y^k)^{D_{n,k}}, \tag{7}$$

which agrees with [11, 12] for $k < 4$ and all weights n, and with available data on MZVs, obtained from binary reshuffles [7] at weights $n \leq 20$ for $k = 4$, and $n \leq 18$ for $k > 4$. Further tests of (7) require very large scale computations, which are in progress, with encouraging results. However, the work reported here does not rely on this conjecture; the values of $\{M_n \mid n \leq 15\}$ in Table 1 are sufficient for present purposes, and these are amply verified by exhaustive use of the integer-relation search routine MPPSLQ [18].

Finally, in this section, we remark on the simplicity of the prediction of (4) for the dimensionality, K_n, of the search space for counterterms that evaluate to MZVs of weight n. Since π^2, with weight $n = 2$, does not occur in such counterterms, it follows that they must be expressible in terms of transcendentals that are enumerated by $\{M_n \mid n \geq 3\}$, and products of such knot-numbers [1, 9, 13]. Thus K_n is given by a Padovan sequence:

$$\sum_n x^n K_n = \frac{x^3}{1 - x^2 - x^3}\,; \quad K_n = K_{n-2} + K_{n-3}\,; \quad K_1 = 0\,; \quad K_2 = 0\,; \quad K_3 = 1\,, \tag{8}$$

which is developed in Table 1. Note that the dimension of the search space for a general MZV of weight n is K_{n+3} [6], which exceeds K_n by a factor [17] of 2.324717957, as $n \to \infty$.

3. Knot-numbers from evaluations of Feynman diagrams

The methods at our disposal [1, 2, 5] do not yet permit us to predict, *a priori*, the transcendental knot-number assigned to a positive knot by field-theory counterterms; instead we need a concrete evaluation of at least one diagram which skeins to produce that knot. Neither do they allow us to predict the rational coefficients with which such knot-numbers, and their products, corresponding to factor knots, occur in a counterterm; instead we must, at present, determine these coefficients by analytical calculation, or by applying a lattice method, such as MPPSLQ [18], to (very) high-precision numerical data. Nonetheless, the consequences of [1, 2] are highly predictive and have survived intensive testing with amazing fidelity. The origin of this predictive content is clear: once a knot-number is determined by one diagram, it is then supposed, and indeed found, to occur in the evaluation of all other diagrams which skein to produce that knot. Moreover, the search space for subdivergence-free counterterms that evaluate to MZVs is impressively smaller than that for the MZVs themselves, due to the absence of any knot associated with π^2, and again the prediction is borne out by a wealth of data.

We exemplify these features by considering diagrams that evaluate to MZVs of depths up to 5, which is the greatest depth that can occur at weights up to 17, associated with knots up to crossing-number 17, obtained from diagrams with up to 10 loops. We follow the economical notation of [3, 4, 5], referring to a vacuum diagram by a so-called angular diagram [3], which results from choosing one vertex as origin, and indicating all vertices that are connected to this origin by dots, after removing the origin and the propagators connected to it. From such an angular diagram one may uniquely reconstruct the original Feynman diagram. The advantage of this notation is that the Gegenbauer-polynomial x-space technique [3] ensures that the maximum depth of sum which can result is the smallest number of propagators in any angular diagram that characterizes the Feynman diagram. Fig. 1 shows a naming convention for log-divergent vacuum diagrams with angular diagrams that yield up to 5-fold sums. To construct, for example, the 7-loop diagram $G(4,1,0)$ one places four dots on line 1 and one dot on line 2. Writing an origin at any point disjoint from the angular diagram, and joining all 6 dots to that origin, one recovers the Feynman diagram in question. Using analytical techniques developed in [3, 4, 12, 13], we find that all subdivergence-free diagrams of G-type, up to 13 loops (the highest number computable in the time available), give counterterms that evaluate to $\zeta(2n+1)$, their products, and depth-3 knot-numbers chosen from the sets

$$\begin{aligned} N_{2m+1,2n+1,2m+1} &= \zeta(2m+1,2n+1,2m+1) - \zeta(2m+1)\,\zeta(2m+1,2n+1) \\ &\quad + \sum_{k=1}^{m-1} \binom{2n+2k}{2k} \zeta_P(2n+2k+1,2m-2k+1,2m+1) \\ &\quad - \sum_{k=0}^{n-1} \binom{2m+2k}{2k} \zeta_P(2m+2k+1,2n-2k+1,2m+1)\,, \qquad (9) \\ N_{2m,2n+1,2m} &= \zeta(2m,2n+1,2m) + \zeta(2m)\,\{\zeta(2m,2n+1) + \zeta(2m+2n+1)\} \\ &\quad + \sum_{k=1}^{m-1} \binom{2n+2k}{2k} \zeta_P(2n+2k+1,2m-2k,2m) \\ &\quad + \sum_{k=0}^{n-1} \binom{2m+2k}{2k+1} \zeta_P(2m+2k+1,2n-2k,2m)\,, \qquad (10) \end{aligned}$$

where $\zeta_P(a,b,c) = \zeta(a)\,\{2\,\zeta(b,c) + \zeta(b+c)\}$. The evaluation of a 9-loop non-planar example, $G(3,2,2)$, is given in [13]: it evaluates in terms of MZVs of weights ranging from 6 to 14. Choosing from (9,10) one knot-number at 11 crossings and two at 13 crossings, one arrives at an expression from which all powers of π^2 are banished, which is a vastly more specific result than for a generic collection of MZVs of these levels, and is in striking accord with what is required by the knot-to-number connection entailed by field theory. Moreover, all planar diagrams that evaluate to MZVs have been found to contain terms purely of weight $2L-3$ at L loops, matching the pattern of the zeta-reducible crossed ladder diagrams [1, 2].

Subdivergence-free counterterms obtained from the M-type angular diagrams of Fig. 1 evaluate to MZVs of weight $2L-4$, at L-loops, with depths up to 4. Up to $L=8$ loops, corresponding to 12 crossings, the depth-4 MZVs can be reduced to the depth-2 alternating sums [13] $N_{a,b} \equiv \zeta(\overline{a},b) - \zeta(\overline{b},a)$. The knot-numbers for the $(4,3)$ and $(5,3)$ torus knots may be taken as $N_{5,3}$ and $N_{7,3}$, thereby banishing π^2 from the associated 6-loop and 7-loop counterterms. In general, $N_{2k+5,3}$ is a $(2k+8)$-crossing knot-number at $(k+6)$ loops. Taking the second knot-number at 12 crossings as [9, 13] $N_{7,5} - \frac{\pi^{12}}{2^5 10!}$, we express all 8-loop M-type counterterms in a π-free form. At 9 loops, and hence 14 crossings, we encounter the first depth-4 MZV that cannot be pushed down to alternating Euler sums of depth 2. The three knot-numbers are again highly specific: to $N_{11,3}$ we adjoin

$$N_{9,5} + \tfrac{5\pi^{14}}{7032946176}\,; \quad \zeta(5,3,3,3) + \zeta(3,5,3,3) - \zeta(5,3,3)\zeta(3) + \tfrac{24785168\pi^{14}}{4331237155245}\,. \tag{11}$$

Having determined these knot-numbers by applying MPPSLQ to 200 significant-figure evaluations of two counterterms, in a search space of dimension $K_{17}=21$, requisite for generic MZVs of weight 14, knot theory requires that we find the remaining five M-type counterterms in a search space of dimension merely $K_{14}=9$. This prediction is totally successful. The rational coefficients are too cumbersome to write here; the conclusion is clear: when counterterms evaluate to MZVs they live in a π-free domain, much smaller than that inhabited by a generic MZV, because of the apparently trifling circumstance that a knot with only two crossings is necessarily the unknot.

Such wonders continue, with subdivergence-free diagrams of types C and D in Fig. 1 Up to 7 loops we have obtained *all* of them in terms of the established knot-numbers $\{\zeta(3),\zeta(5),\zeta(7),N_{5,3},\zeta(9),N_{7,3},\zeta(11),N_{3,5,3}\}$, associated in [5, 9] with the positive knots $\{(3,2),(5,2),(7,2),8_{19}=(4,3),(9,2),10_{124}=(5,3),(11,2),11_{353}=\sigma_1\sigma_2^3\sigma_3^2\sigma_1^2\sigma_2^2\sigma_3\}$, and products of those knot-numbers, associated with the corresponding factor knots. A non-planar L-loop diagram may have terms of different weights, not exceeding $2L-4$. Invariably, a planar L-loop diagram evaluates purely at weight $2L-3$. Hence we expect the one undetermined MZV knot-number at 15 crossings to appear in, for example, the planar 9-loop diagram $C(1,0,4,0,1)$. To find the precise combination of $\zeta(9,\overline{3},\overline{3}) - \frac{3}{14}\zeta(7,\overline{5},\overline{3})$ with other Euler sums would require a search in a space of dimension $K_{18}=28$. Experience suggests that would require an evaluation of the diagram to about 800 sf, which is rather ambitious, compared with the 200 sf which yielded (11). Once the number is found, the search space for further counterterms shrinks to dimension $K_{15}=12$.

4. Positive knots associated with irreducible MZVs

Table 2 gives the braid words [16] of 5 classes of positive knot. For each type of knot, $\mathcal{K}$, we used the skein relation to compute the HOMFLY polynomial [16], $X_{\mathcal{K}}(q,\lambda)$, in terms of $p_n = (1-q^{2n})/(1-q^2)$, $r_n = (1+q^{2n-1})/(1+q)$, $\Lambda_n = \lambda^n(1-\lambda)(1-\lambda q^2)$.

Table 2: Knots and HOMFLY polynomials associated with irreducibles MZVs.

$\mathcal{K}$	$X_{\mathcal{K}}(q,\lambda)$
$\mathcal{T}_{2k+1} = \sigma_1^{2k+1}$	$T_{2k+1} = \lambda^k(1+q^2(1-\lambda)p_k)$
$\mathcal{R}_{k,m} = \sigma_1\sigma_2^{2k+1}\sigma_1\sigma_2^{2m+1}$	$R_{k,m} = T_{2k+2m+3} + q^3 p_k p_m \Lambda_{k+m+1}$
$\mathcal{R}_{k,m,n} = \sigma_1\sigma_2^{2k}\sigma_1\sigma_2^{2m}\sigma_1\sigma_2^{2n+1}$	$R_{k,m,n} = R_{1,k+m+n-1} + q^6 p_{k-1}p_{m-1}r_n\Lambda_{k+m+n+1}$
$\mathcal{S}_k = \sigma_1\sigma_2^3\sigma_3^2\sigma_1^2\sigma_2^{2k}\sigma_3$	$S_k = T_3^2 T_{2k+3} + q^2 p_k r_2 (q^2(\lambda-2)+q-2)\Lambda_{k+3}$
$\mathcal{S}_{k,m,n} = \sigma_1\sigma_2^{2k+1}\sigma_3\sigma_1^{2m}\sigma_2^{2n+1}\sigma_3$	$S_{k,m,n} = T_{2k+2m+2n+3} + q^3(p_kp_m + p_mp_n + p_np_k$ $+ (q^2(3-\lambda)-2q)p_kp_mp_n)\Lambda_{k+m+n+1}$

Noting that $\mathcal{S}_{1,1,1} = \mathcal{S}_1$ and $\mathcal{S}_{m,n,0} = \mathcal{R}_{m,n,0} = \mathcal{R}_{m,n}$, one easily enumerates the knots of Table 2. The result is given, up to 17 crossings, in the last row of Table 3, where it is compared with the enumeration of all prime knots, which is known only to 13 crossings, and with the enumeration of positive knots, which we have achieved to 15 crossings, on the assumption that the HOMFLY polynomial has no degeneracies among positive knots. It is apparent that positive knots are sparse, though they exceed the irreducible MZVs at 10 crossings and at all crossing numbers greater than 11. The knots of Table 2 are equal in number to the irreducible MZVs up to 16 crossings; thereafter they are deficient. Table 4 records a finding that may be new: the Alexander polynomial [16], obtained by setting $\lambda = 1/q$ in the HOMFLY polynomial, is not faithful for positive knots. The Jones polynomial [16], with $\lambda = q$, was not found to suffer from this defect. Moreover, by using REDUCE [19], and assuming the fidelity of the HOMFLY polynomial in the positive sector, we were able to prove, by exhaustion, that none of the $4^{14} \approx 2.7 \times 10^8$ positive 5-braid words of length 14 gives a true 5-braid 14-crossing knot.

Table 3: Enumerations of classes of knots by crossing number, n, compared with (4).

n	3	4	5	6	7	8	9	10	11	12	13	14	15	16	17
prime knots	1	1	2	3	7	21	49	165	552	2176	9988	?	?	?	?
positive knots	1	0	1	0	1	1	1	3	2	7	9	17	47	?	?
M_n	1	0	1	0	1	1	1	1	2	2	3	3	4	5	7
Table 2 knots	1	0	1	0	1	1	1	1	2	2	3	3	4	5	5

Table 4: Pairs of positive knots with the same Alexander polynomial, $X_{\mathcal{K}}(q,1/q)$.

$\mathcal{K}_1$	$\mathcal{K}_2$	$X_{\mathcal{K}_1}(q,\lambda) - X_{\mathcal{K}_2}(q,\lambda)$
$\mathcal{S}_{2,1,2} = \sigma_1\sigma_2^5\sigma_3\sigma_1^2\sigma_2^5\sigma_3$	$\sigma_1^3\sigma_2^4\sigma_3\sigma_1^2\sigma_2^2\sigma_3^2\sigma_2$	$q^4(1-\lambda q)p_2r_2\Lambda_6$
$(\sigma_1\sigma_2^2\sigma_3)^2\sigma_1\sigma_2^5\sigma_3$	$(\sigma_1\sigma_2^2\sigma_3)^2\sigma_1^3\sigma_2\sigma_1^2\sigma_3$	$q^5(1-\lambda q)p_2\Lambda_6$
$\sigma_1^5\sigma_2\sigma_3\sigma_1^2\sigma_2^3\sigma_3^2\sigma_2$	$\sigma_1^2\sigma_2^2\sigma_1^3\sigma_2^7$	$q^5(1-\lambda q)p_2\Lambda_6$

The association [1, 2] of the 2-braid torus knots $(2k+1,2) = \mathcal{T}_{2k+1}$ with the transcendental numbers $\zeta(2k+1)$ lies at the heart of our work. In [2, 5], we associated the 3-braid torus knot $(4,3) = 8_{19} = \mathcal{R}_{1,1}$ with the unique irreducible MZV at weight 8, and

in [5] we associated $(5,3) = 10_{124} = \mathcal{R}_{2,1}$ with that at weight 10. The 7-loop counterterms of ϕ^4-theory indicate that the knot-numbers associated with $10_{139} = \sigma_1\sigma_2^3\sigma_1^3\sigma_2^3$ and $10_{152} = \sigma_1^2\sigma_2^2\sigma_1^3\sigma_2^3$ are not [5] MZVs. At 11 crossings, the association of the knot-number $N_{3,5,3}$ with $\mathcal{S}_1 = \mathcal{S}_{1,1,1} \equiv 11_{353}$ is rock solid: we have obtained this number analytically from 2 diagrams and numerically from another 8, in each case finding it with different combinations of $\zeta(11)$ and the factor-knot transcendental $\zeta^2(3)\zeta(5)$. In [9] we associated the family of knots $\mathcal{R}_{k,m}$ with the knot-numbers $N_{2k+3,2m+1}$, modulo multiples of $\pi^{2k+2m+4}$ that have now been determined up to 14 crossings. It therefore remains to explain here how: (a) two families of 4-braids, $\mathcal{S}_k$ and $\mathcal{S}_{k,m,n}$, diverge from their common origin at 11 crossings, to give two knots at 13 crossings, and three at 15 crossings, associated with triple Euler sums; (b) a new family, $\mathcal{R}_{k,m,n}$, begins at 14 crossings, giving the $(7,3)$ torus knot, $(\sigma_1\sigma_2)^7 = (\sigma_1\sigma_2^4)^2\sigma_1\sigma_2^3 = \mathcal{R}_{2,2,1}$, associated with a truly irreducible four-fold sum.

To relate the positive knots of Table 2 to Feynman diagrams that evaluate to MZVs we shall dress their braid words with chords. In each of Figs. 2–8, we proceed in two stages: first we extract, from a braid word, a reduced Gauss code that defines a trivalent chord diagram; then we indicate how to shrink propagators to obtain a scalar diagram that is free of subdivergences and has an overall divergence that evaluates to MZVs. Our criterion for reducibility to MZVs is that there be an angular diagram, obtained [3, 4] by choosing one vertex as an origin, such that the angular integrations may be performed without encountering 6–j symbols, since these appeared in all the diagrams involving the non-MZV knots 10_{139} and 10_{152} at 7 loops [5], whereas all the MZV-reducible diagrams could be cast in a form free of 6–j symbols.

The first step – associating a chord diagram with a knot – allows considerable freedom: each chord is associated with a horizontal propagator connecting vertical strands of the braid between crossings, and there are almost twice as many crossings as there are chords in the corresponding diagram. Moreover, there are several braid words representing the same knot. Thus a knot can be associated with several chord diagrams. Figs. 3b and 4b provide an example: each diagram obtained from the $(5,2)$ torus knot yields a counterterm involving $\zeta(5)$, in a trivalent theory such as QED or Yukawa theory.

In Table 2 we have five families of braid words: the 2-braid torus knots, two families of 3-braids, and two families of 4-braids. We begin with the easiest family, $\mathcal{T}_{2k+1}$. Consider Fig. 2a. We see the braid σ_1^3, dressed with two horizontal propagators. Such propagators will be called chords, and we shall refer to Figs. 2a–8a as chorded braid diagrams. In Fig. 2a the two chords are labelled 1 and 2. Following the closed braid, starting from the upper end of the left strand, we encounter each chord twice, at vertices which we label $\{1,1'\}$ and $\{2,2'\}$. These occur in the order $1,2,1',2'$ in Fig. 2a. This is the same order as they are encountered on traversing the circle of Fig. 2b, which is hence the same diagram as the chorded braid of Fig. 2a. As a Feynman diagram, Fig. 2b is indeed associated with the trefoil knot, by the methods of [1]. We shall refer to the Feynman diagrams of Figs. 2b–8b as chord diagrams[1]. Each chord diagram is merely a rewriting of the chorded braid diagram that precedes it, displaying the vertices on a hamiltonian circuit that passes through all the vertices. The final step is trivial in this example: the scalar

[1]The reader familiar with recent developments in knot theory and topological field theory might notice that our notation is somewhat motivated by the connection between Kontsevich integrals [7] and chord diagrams. In [15] this will be discussed in detail and related to the work in [1].

tetrahedron is already log-divergent in 4 dimensions, so no shrinking of propagators is necessary. Fig. 2c records the trivial angular diagram, obtained [3] by choosing 2 as an origin and removing the propagators connected to it: this merely represents a wheel with 3 spokes. In general [4] the wheel with $n+1$ spokes delivers $\zeta(2n-1)$.

In Fig. 3a we give a chording of the braid σ_1^{2n-1}, which is the simplest representation of the $(2n-1,2)$ torus knot, known from previous work [1, 2] to be associated with a $(n+1)$-loop diagram, and hence with a hamiltonian circuit that has n chords. Thus each addition of σ_1^2 involves adding a single chord, yielding the chord diagram of Fig. 3b. To obtain a logarithmically divergent scalar diagram, we shrink the propagators connecting vertex $2'$ to vertex n', drawn with a thick line on the hamiltonian circuit of Fig. 3b, and hence obtain the wheel with $n+1$ spokes, represented by the angular diagram of Fig. 3c.

To show how different braid-word representations of the same knot give different chord diagrams, yet the same transcendental, we consider Fig. 4. In Fig. 4a we again have a chorded braid with n chords, which this time is obtained by combining $\sigma_1\sigma_2\sigma_1\sigma_2$ with $n-2$ powers of σ_2^2. The resultant braid word, $\sigma_1\sigma_2\sigma_1\sigma_2^{2n-3}$, is the $(2n-1,2)$ torus knot written as a 3-braid. Labelling the pairs of vertices of Fig. 4b, one sees that it is identical to the closure of the braid of Fig. 4a. Shrinking together the vertices $\{2', n', \ldots, 3'\}$ gives the angular diagram of Fig. 4c, which is the same as Fig. 3c and hence delivers $\zeta(2n-1)$.

This ends our consideration of the 2-braid torus knots. We now turn to the class $\mathcal{R}_{k,m}$ in Fig. 5. The first member $\mathcal{R}_{1,1} = 8_{19} = (4,3)$ appears at 6 loops, with five chords. It was obtained from Feynman diagrams in [2], and found in [5] to be associated with an MZV of depth 2. In Fig. 5a we add singly-chorded powers of σ_2^2 to a chorded braid word that delivers a Feynman diagram for which the procedures of [1] gave 8_{19} as one of its skeinings. In general, we have $k+m+3$ chords and thus $k+m+4$ loops. The resulting chord diagram is Fig. 5b, whose 7-loop case was the basis for associating 10_{124} with the MZV $\zeta(7,3)$ [5]. Shrinking the propagators indicated by thickened lines in Fig. 5b, we obtain diagram $M(k,1,1,m)$, indicated by the angular diagram of Fig. 5c. Explicit computation of all such diagrams, to 9 loops, shows that this family is indeed MZV-reducible, to 14 crossings.

In Fig. 6 we repeat the process of Fig. 5 for the knot class $\mathcal{R}_{k,m,n}$. Marked boxes, in Fig. 6a, indicate where we increase the number of chords. Fig. 6b shows the highly non-planar chord diagram for this knot class. This non-planarity is maintained in the log-divergent diagram obtained by shrinking the thickened lines in Fig. 6b. The parameters m and k correspond to the series of dots in the corresponding angular diagram of Fig. 6c. Non-planarity is guaranteed by the two remaining dots, which are always present. For $n > 1$, we see even more propagators in the angular diagram. The absence of 6–j symbols from angular integrations leads us to believe that the results are reducible to MZVs; the non-planarity entails MZVs of even weight, according to experience up to 7 loops [5].

We now turn to the last two classes of knots: the 4-braids of Table 2. In Fig. 7a we give a chorded braid diagram for knots of class $\mathcal{S}_k$. Again, the marked box indicates how we add chords to a chorded braid diagram that corresponds to a 7-loop Feynman diagram, already known [5] to skein to produce $\mathcal{S}_1 = 11_{353}$. Shrinking the thickened lines in Fig. 7b, we obtain a log-divergent planar diagram containing: a six-point coupling, a $(k+3)$-point coupling, and $k+5$ trivalent vertices. This is depicted in Fig. 7c as an angular diagram obtained by choosing the $(k+3)$-point coupling as an origin. Choosing

the 6-point coupling as an origin for the case $k = 1$ confirms that $\mathcal{S}_1 = 11_{353}$ is associated with $\zeta(3, 5, 3)$ via the 7-loop diagram $G(4, 1, 0)$. However, for $k = 3$ there is no way of obtaining MZVs of depth 3 from either choice of 6-point origin. Hence we expect a depth-5 MZV to be associated with the 15-crossing knot $\mathcal{S}_3$, with the possibility of depth-7 MZVs appearing at higher crossings.

Finally we show that the three-parameter class $\mathcal{S}_{k,m,n}$, also built on $11_{353} = \mathcal{S}_{1,1,1}$, is associated with depth-3 MZVs. The chorded braid of Fig. 8a indicates the three places where we can add further chords. Fig. 8b gives the chord diagram associated with it, and indicates how to shrink propagators to obtain a log-divergent diagram, represented by the angular diagram $G(m + n + 2, k, 0)$ of Fig. 8c, which evaluates in terms of depth-3 MZVs up to 13 loops, and presumably beyond.

5. Conclusions

In summary, we have

1. enumerated in (3,4) the irreducibles entailed by Euler sums and multiple zeta values at weight n; apportioned them by depth in (6); conjectured the generator (7) for the number, $D_{n,k}$, of MZVs of weight n and depth k that are irreducible to MZVs of lesser depth;

2. determined all MZV knot-numbers to 15 crossings, save one, associated with a 9-loop diagram that evaluates to MZVs of depth 5 and weight 15;

3. enumerated positive knots to 15 crossings, notwithstanding degenerate Alexander polynomials at 14 and 15 crossings;

4. developed a technique of chording braids so as to generate families of knots founded by parent knots whose relationship to Feynman diagrams was known at lower loop numbers;

5. combined all the above to identify, in Table 2, knots whose enumeration, to 16 crossings, matches that of MZVs.

Much remains to be clarified in this rapidly developing area. Positive knots, and hence the transcendentals associated with them by field theory, are richer in structure than MZVs: there are more of them than MZVs; yet those whose knot-numbers are MZVs evaluate in search spaces that are significantly smaller than those for the MZVs, due to the absence of a two-crossing knot. After 18 months of intense collaboration, entailing large scale computations in knot theory, number theory, and field theory, we are probably close to the boundary of what can be discovered by semi-empirical methods. The trawl, to date, is impressive, to our minds. We hope that colleagues will help us to understand it better.

Acknowledgements We are most grateful to Don Zagier for his generous comments, which encouraged us to believe in the correctness of our discoveries (6), while counselling caution as to the validity of (7) in so far uncharted territory with depth $k > 4$. David Bailey's MPPSLQ [18], Tony Hearn's REDUCE [19] and Neil Sloane's superseeker [20] were instrumental in this work. We thank Bob Delbourgo for his constant encouragement.

References

[1] D. Kreimer, Habilitationsschrift: *Renormalization and Knot Theory*, Mainz preprint MZ–TH–96–18 (July 1996), to appear in Journal of Knot Theory and its Ramifications; q-alg/9607022.

[2] D. Kreimer, Phys. Lett. **B354** (1995) 117.

[3] K.G. Chetyrkin, A.L. Kataev and F.V. Tkachov, Nucl. Phys. **B174** (1980) 345; H. Kleinert, J. Neu, V. Schulte-Frohlinde, K.G. Chetyrkin and S.A. Larin, Phys. Lett. **B272** (1991) 39; **B319** (1993) 545 (erratum).

[4] D.J. Broadhurst, Open University report OUT-4102-18 (1985); Phys. Lett. **B164** (1985) 356; Z. Phys. **C32** (1986) 249; Phys. Lett. **B307** (1993) 132; D.T. Barfoot and D.J. Broadhurst, Z. Phys. **C41** (1988) 81.

[5] D.J. Broadhurst and D. Kreimer, Int. J. Mod. Phys. **C6** (1995) 519.

[6] D. Zagier, in Proc. First European Congress Math. (Birkhäuser, Boston, 1994) Vol II, pp 497-512; *Multiple Zeta Values*, in preparation.

[7] T.Q.T. Le and J. Murakami, MPI Bonn preprints 93-26; 93-89 (1993); C. Kassel, *Quantum groups* (Springer, New York, 1995) pp 480-483.

[8] D.J. Broadhurst, R. Delbourgo and D. Kreimer, Phys. Lett. **B366** (1996) 421.

[9] D.J. Broadhurst, J.A. Gracey and D. Kreimer, Open University preprint, OUT–4102–46 (1996); hep-th/9607174, to appear in Z. Phys. C.

[10] R. Delbourgo, A. Kalloniatis and G. P. Thompson, Phys. Rev. **D54** (1996) 5373.

[11] D. Borwein, J.M. Borwein and R. Girgensohn, Proc. Edin. Math. Soc. **38** (1995) 273.

[12] J. M. Borwein and R. Girgensohn, Electronic J. Combinatorics **3** (1996) R23, with an appendix by D. J. Broadhurst.

[13] D.J. Broadhurst, Open University preprint, OUT–4102–62 (1996); hep-th/9604128, to appear in J. Math. Phys.

[14] J.M. Borwein, D.A. Bradley and D.J. Broadhurst, Open University preprint, OUT–4102–63 (1996); hep-th/9611004, to appear in Electronic J. Combinatorics.

[15] D. Kreimer, *Knots and Feynman Diagrams* (Cambridge University Press, in preparation).

[16] V.F.R. Jones, Annals of Math. **126** (1987) 335.

[17] W. Adams and D. Shanks, Math. Comp. **39** (1982) 255.

[18] D. H. Bailey, ACM Trans. Math. Software **21** (1995) 379.

[19] A.C. Hearn, REDUCE user's manual, version 3.5, Rand publication CP78 (1993).

[20] N. J. A. Sloane, Electronic J. Combinatorics **1** (1994) F1.

Fig. 1: Angular diagrams yielding MZVs of depths up to 5.

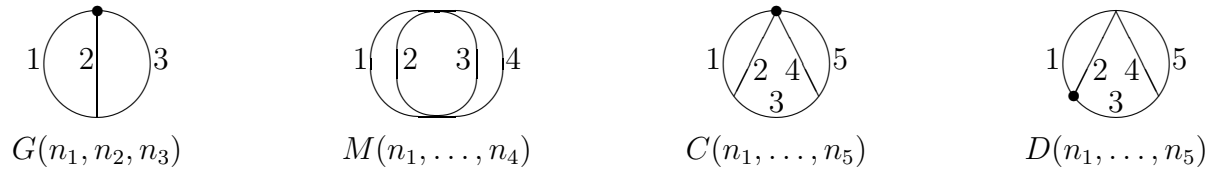

$G(n_1, n_2, n_3)$ $M(n_1, \ldots, n_4)$ $C(n_1, \ldots, n_5)$ $D(n_1, \ldots, n_5)$

Fig. 2: The lowest level non-trivial chorded braid appears at three loops, and is given in (a). It is the same Feynman diagram as the chord diagram in (b), and gives rise to the simple angular diagram of (c). In (a) we indicate the closure of the braid by dotted lines, which we omit from subsequent figures.

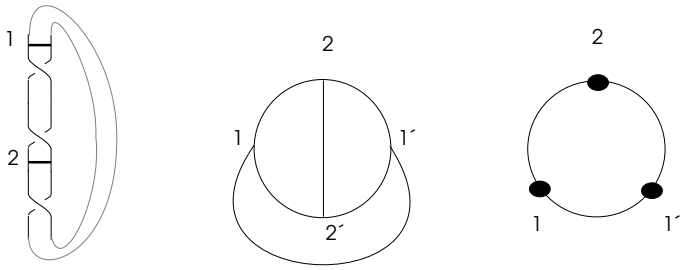

Fig. 3: We extend Fig. 2 to produce the chorded braid (a) and the chord diagram (b), which deliver $\zeta(2n-1)$ from the angular diagram of (c). The thick line is shrunk to a point to produce a $(n+1)$-point vertex, serving as the origin in (c).

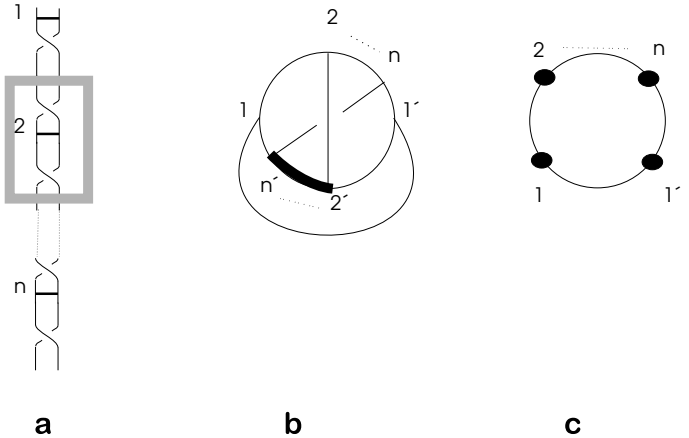

Fig. 4: The braid in (a) is a 3-braid representation for the $(2, 2n-1)$ torus knot. It produces an angular diagram (c) that is the same as in Fig. 3, after shrinking the thickened line in (b).

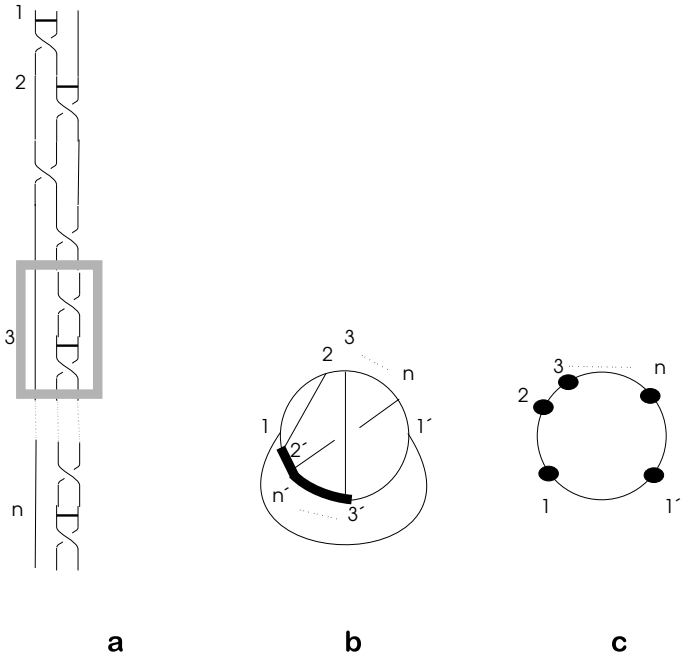

Fig. 5: In this genuine 3-braid example, the chorded braid (a) is equivalent, as a Feynman diagram, to the chord diagram (b), and gives rise to the class $M(k, 1, 1, m)$ of angular diagrams in (c), by shrinking: two vertices to a 4-point vertex at the top of the diagram in (b); the propagator $(1, 1')$ to a 4-point vertex; and $k+m$ vertices to a $(k+m+2)$-point vertex, which then serves as the origin in (c).

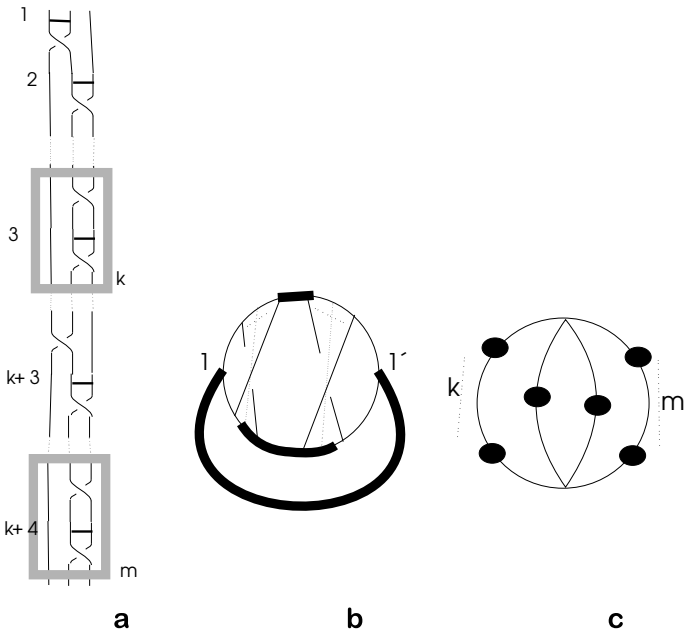

Fig. 6: Another genuine class of 3-braids, which we believe to entail MZVs of even weight. We obtain two 4-point vertices by shrinking the indicated thick lines at the top and right of the circle in (b). We further shrink $k+m$ vertices at the bottom, and $n+1$ vertices at the left, to obtain an angular diagram (c) that is free of 6–j symbols.

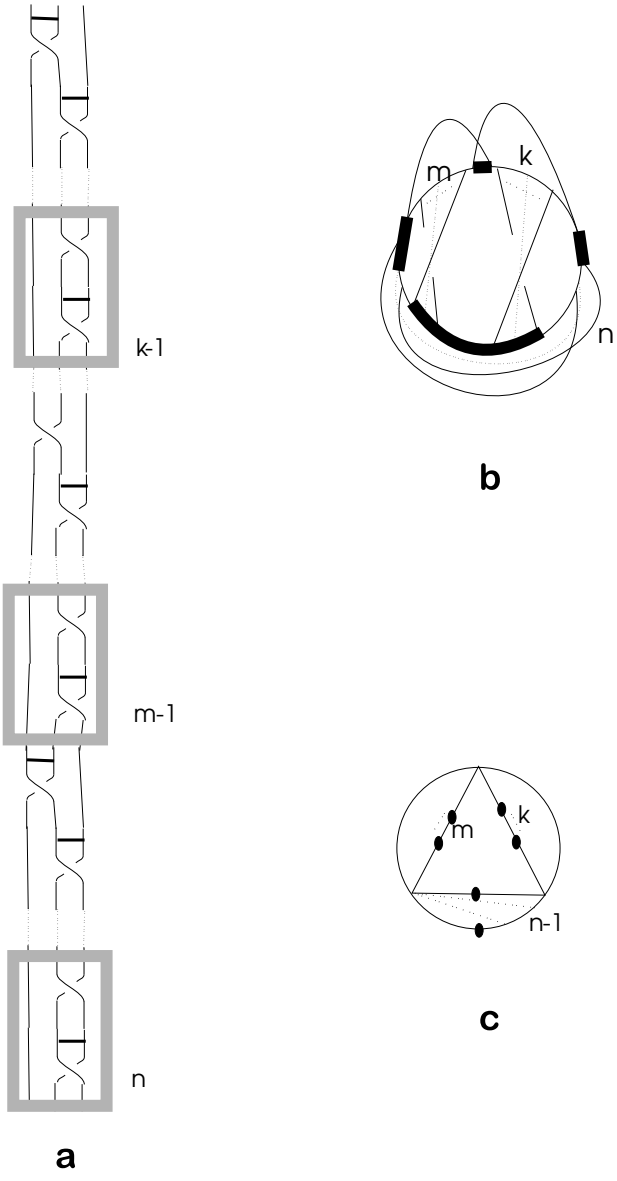

Fig. 7: This shows the first class of genuine 4-braids, which gives rise to a planar angular diagram, beginning with 11_{353}, for $k = 1$. We shrink four vertices at the top, and $k + 1$ vertices at the right, as indicated in (b).

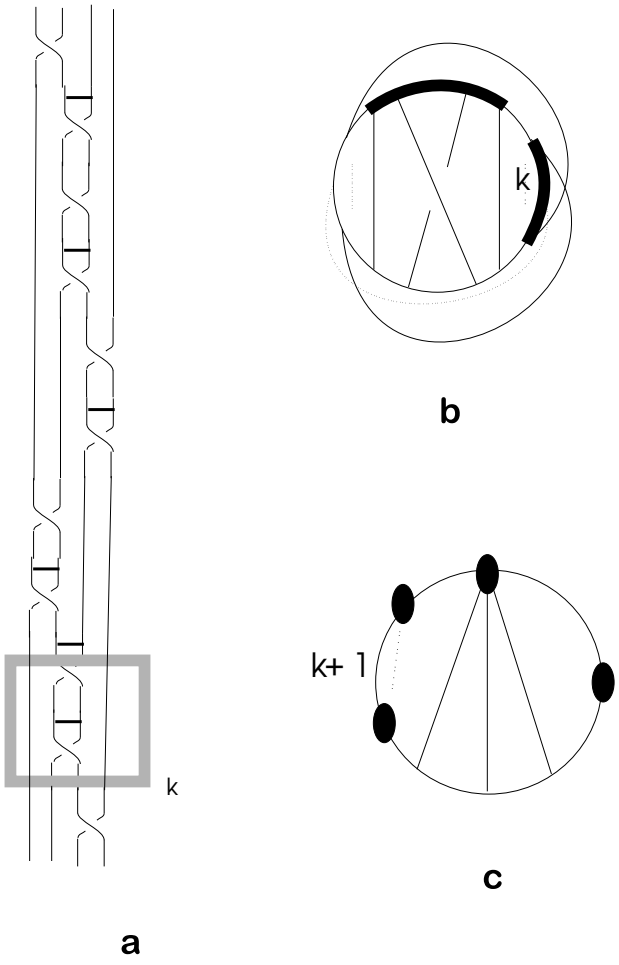

Fig. 8: This triple-index class of 4-braids also begins with 11_{353}, for $k = m = n = 1$. From shrinking, we obtain a 4-point vertex at the left of (b), and at the bottom a $(m+n+k+3)$-point vertex that is the origin of the planar angular diagram $G(m + n + 2, k, 0)$ of (c).